Journal of the Taiwan Institute of Chemical Engineers 138 (2022) 104448

Contents lists available at ScienceDirect

Journal of the Taiwan Institute of Chemical Engineers

journal homepage: www.journals.elsevier.com/journal-of-the-taiwan-institute-of-chemical-engineers

Electrochemical cleaning of superhydrophobic polyvinylidene fluoride/polymethyl methacrylate/carbon black membrane after membrane distillation

N.A. Zakaria [a], S.Q. Zaliman [a], C.P. Leo [a,*], A.L. Ahmad [a], B.S. Ooi [a], Phaik Eong Poh [b]

[a] School of Chemical Engineering, Engineering Campus, Universiti Sains Malaysia, 14300, Nibong Tebal, Pulau Pinang, Malaysia
[b] Chemical Engineering Discipline, School of Engineering, Monash University Malaysia, Jalan Lagoon, 47500, Bandar Sunway, Selangor, Malaysia

ARTICLE INFO

Keywords:
PVDF
Membrane distillation
Carbon black
PMMA
Electrochemical cleaning

ABSTRACT

In membrane distillation, separation can be greatly enhanced by the use of membranes with high porosity and hydrophobic surface. However, their separation performance drops significantly due to wetting in the presence of surfactant. In this work, polymethyl methacrylate (PMMA), carbon black and/or conductive ink was incorporated into PVDF membranes with microroughness templated from weave pattern to improve membrane morphology electrochemical properties. Fourier transform infrared spectra showed characteristic peaks of PVDF and additives. Carbon black and conductive ink caused the formation of secondary roughness, while PMMA induced high porosity and thickness. The PVDF-PMMA-CB membrane with a superhydrophobic surface also attained electrical conductivity with cyclic voltammetry recorded. A high permeate flux and stable salt rejection were achieved using this membrane in membrane distillation. It could also be electrochemically cleaned within 4 min after wetting by surfactant, showing a recovered water contact angle of 148.8 °. The membrane could be cleaned by hypochlorite (OCl−), hypochlorous acid (HOCl), and/or ferric hydroxides generated during electrochemical cleaning. The cleaned PVDF-PMMA-CB membrane achieved NaCl rejection of more than 95%, but a slightly lower permeate flux than the permeate flux before wetting.

1. Introduction

Water scarcity affects the sustainable growth of our economy and society unless we can improve the water recovery technologies. In recent years, membrane distillation received more attention than other water recovery technologies because it allows the recovery of water from different water resources using low-grade heat sources without using high pressure.

The hydrophobic polyvinylidene fluoride (PVDF) membranes with macropores remain popular in membrane distillation as they can be easily fabricated through phase inversion or electrospinning. Besides improving surface hydrophobicity through different strategies to prevent wetting [1], they were modified to achieve high porosity to promote the permeation of water vapour [2]. They were blended with different polymers with varied miscibility to disturb demixing during phase inversion, exhibiting negative heat of mixing if miscible [3–6]. The changes in system thermodynamics could affect pore formation. The blending polymethyl methacrylate (PMMA) into PVDF dope solution resulted in an increased BSA rejection and porosity with a reduced water contact angle [7]. The pore size was further reduced after thermally induced phase inversion, which involved casting at -30°C followed by an icy water bath [8]. Together with poly(L-lactic acid), PMMA could also serve as the template to improve the porosity of the PVDF membrane through chloroform etching [8]. Nanopores formed, and the surface roughness increased to enhance the water contact angles. PVDF could also be anchored on PMMA strongly during electrospinning [9]. The electrospun PVDF membrane on PMMA/polyacrylonitrile nanofiber support achieved a water contact angle of 131 ° and removed water from methylbenzene effectively. PMMA also improved the conductivity of PVDF film blended with $LiClO_4$ because of the improvement of charge carriers' mobility [10]. The ionic conductivity of the PVDF/PMMA membrane increased because of the increasing electrolyte uptake into the porous structure and the presence of PMMA [11]. More additives such as palygorskite modified PMMA [12] and PMMA-co-poly (chloromethyl styrene) [13] could improve the ionic conductivity of PVDF membranes by reducing PVDF crystallinity.

* Corresponding author.
E-mail address: chcpleo@usm.my (C.P. Leo).

https://doi.org/10.1016/j.jtice.2022.104448
Received 31 March 2022; Received in revised form 23 May 2022; Accepted 4 July 2022
Available online 11 July 2022

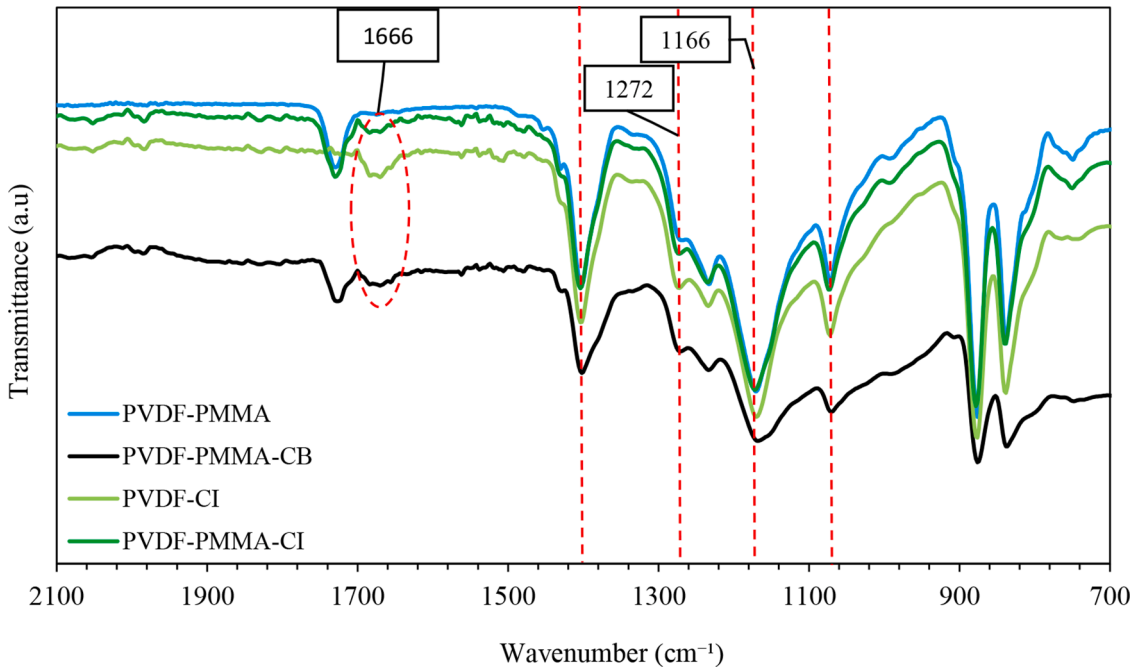

Fig. 1. FTIR spectra of the PVDF membranes with PMMA, carbon black, or conductive ink.

The improvement of membrane conductivity for fouling reduction and membrane cleaning was also reported. The polymeric spacer coated with carbon ink containing graphene nanoplates facilitated the electrocleaning of the PVDF membrane [14]. The membrane was successfully cleaned by hydrogen bubbles formed throughout the microfiltration of sodium alginate suspension in a filtration system incorporated with a graphite electrode (anode) at -0.81 V. The PVDF hollow fiber membrane incorporated with carbon nanotubes was successfully applied in the aerobic and anaerobic wastewater treatment system with a flux recovery of 92% between 0.5 and 1.5 V [15]. Electrochemical cleaning also worked effectively on protein fouled graphene hydrogel membrane. A flux recovery of 99.0 ± 0.1% was recorded after electrochemical cleaning with 0.1 M Na_2SO_4 solution at 1.0 V for 60 min [16]. Small fouling compounds, including dyes on PVDF membrane coated with CNT and reduced graphene oxide, could be electrochemically cleaned at 2.5 V [17]. A very high flux recovery of 94% was attained within 20 min. Besides carbon, the conductive polypyrrole membrane formed on stainless steel through electrochemical polymerization. The membrane was further electrochemically cleaned after being fouled by sodium alginate, BSA, or humic acid [18]. The electronegativity and hydrophilicity of polypyrrole were enhanced under 2.0 V, leading to the successful cleaning.

In this work, PMMA was used to improve the morphology and electrochemical properties of PVDF membranes produced from phase inversion and templating. Carbon black or commercial conductive ink was also blended into PVDF/PMMA membrane. The modified membranes were characterized and tested in membrane distillation. The membranes were fouled by surfactant and then electrochemically cleaned to restore the surface hydrophobicity.

2. Materials and methods

2.1. Materials

The membrane dope solution was prepared using PVDF (Solef ® 6010 powder, Solvay Solexis, France) with a molecular weight in the range of 300-320 kDa as the primary polymer, while N-methyl-2-pyrrolidone (NMP) (>99.5%, Merck, Germany) as the solvent. Polymethyl methacrylate (PMMA) with a molecular weight of 120,000 Da was obtained from Sigma-Aldrich. Carbon black (N220) from the School of Material and Mineral Resources, Universiti Sains Malaysia, and a commercial conductive ink (Bare Conductive, United Kingdom) comprising carbon black, graphite, natural resin, and humectant were selected as the conductive materials. Sodium chloride (NaCl) (>99.5%) and sodium dodecyl sulfate (SDS) (>97%) supplied by Sigma-Aldrich were used to prepare the feed solution of membrane distillation and electrochemical cleaning.

2.2. Synthesis and modification of membrane

PVDF membrane was fabricated through surface templating and phase inversion, as reported elsewhere [19]. PVDF (15 wt.%) was slowly dissolved into NMP at 60 °C under stirring for 6 h to form a PVDF dope solution. For PVDF/PMMA dope solution, 2 wt% of PMMA was added into the PVDF dope solution. Meanwhile, 3 wt% of commercial conductive ink was added to the PVDF dope solution to form the PVDF-CI dope solution. For PVDF-PMMA-CB and PVDF-PMMA-CI dope solutions, 2 wt% of PMMA and 3 wt% of conductive materials (carbon black or commercial conductive ink) were added to the dope solution. An automated casting machine (XB320D, Beijing Jiahang Technology Co. Ltd., China) was used to facilitate the casting with a casting gap of 400 μm. The wet film was precipitated in a coagulation bath containing distilled water for 24 h and dried for another 24 h at room temperature before peeling off from the nonwoven support. Microroughness on the membrane surface was created due to the imprinting effects of the weave pattern on nonwoven support [19].

2.3. Membrane characterization

Fourier transform infrared (FTIR) spectra were scanned using a spectroscope from 600 cm-1 to 3800 cm-1 (Nicolet iS10, Thermo Scientific, USA). A scanning electron microscope (SEM, TM3000, Hitachi, Japan) was utilized to study the surface morphology and cross-section of the fabricated membrane in this work. The surface roughness of membranes was measured using an atomic force microscope (AFM, Hitachi SPA 300HV). The water contact angle on the membrane surface was measured using the image of a water droplet (10 μl) placed on the membrane surface. The water droplet images were captured using the

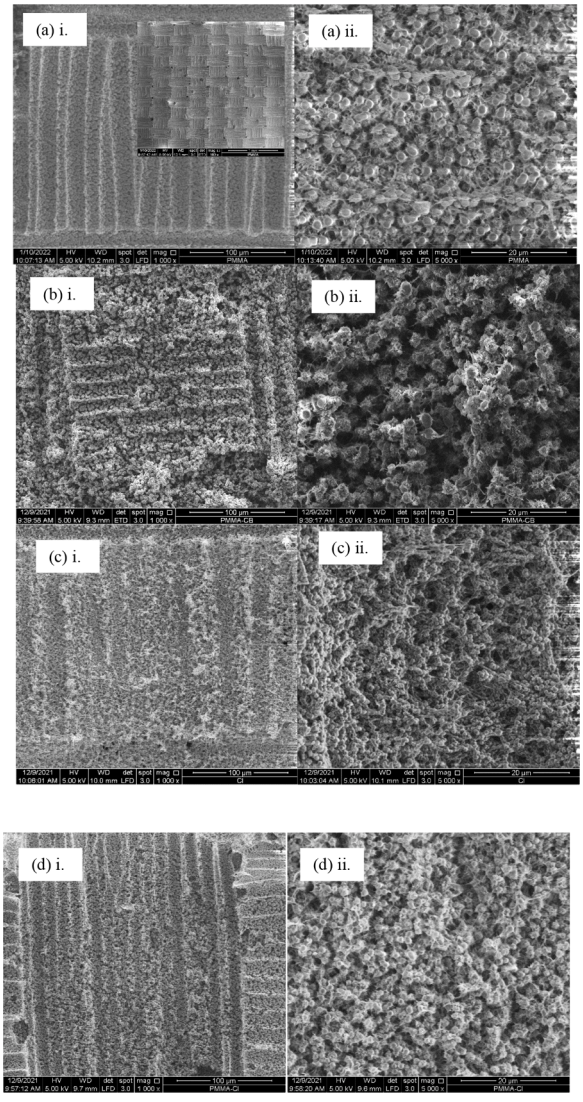

Fig. 2. SEM images showing the surface of (a) PVDF-PMMA, (b) PVDF-PMMA-CB, (c) PVDF-CI, and (d) PVDF-PMMA-CI membranes.

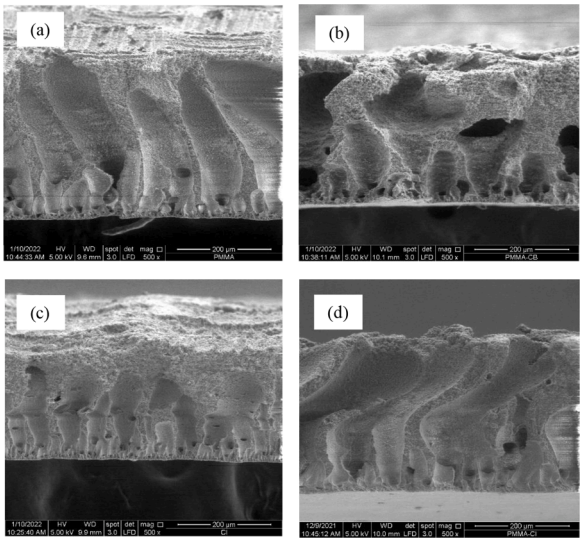

Fig. 3. SEM images showing the cross-section of (a) PVDF-PMMA, (b) PVDF-PMMA-CB, (c) PVDF-CI, and (d) PVDF-PMMA-CI membranes.

electronic microscope (1000X Electronic Digital Microscope Handheld USB Magnifier) and analyzed using ImageJ software. Meanwhile, the sliding angle was measured using a contact angle goniometer (LSA 200, Lauda). The mean pore size of membranes was measured using a gas-liquid displacement porometer (Porolux 1000, IB-FT GmbH, Germany). Before measurement, the membranes were immersed in a wetting agent (Porefil) for 30 min. Membrane porosity ε (%) was calculated from the wet weight and dry weight. The wet weight was obtained from the membrane (3 cm × 1 cm) wetted with 2-butanol, while the dry weight was obtained from the membrane dried at 40 °C.

$$\varepsilon = \frac{m_b/\rho_b}{m_b/\rho_b + m_m/\rho_m} \times 100\% \quad (1)$$

where m_b is the weight of wet membrane (g), m_m is the weight of dry membrane (g), ρ_b is the density of 2-butanol (0.81 g/cm^3), and ρ_m is PVDF density (1.78 g/cm^3). The membrane conductivity was measured using a multimeter (Projecta, DT-830B Digital Multimeter). The conductive membrane was further studied using a potentiostat (Metrohm, μStat 300, Spain). The cyclic voltammetry (CV) test was conducted using phosphate buffer solution (0.05 M) with a scanning range of -0.5 to +1.2 V and a scanning rate of 0.01 V/s.

2.4. Direct contact membrane distillation (DCMD) performance test

The separation performance of membranes was compared using a direct contact membrane distillation (DCMD) system, as described previously [20]. The membrane sample with an effective area of 0.001 m^2 was fixed in a membrane module, separating the hot feed from the cold permeate. The hot feed was the saline solution with 35 g/L of NaCl at 60 ± 2 °C and the cold permeate was the distilled water at 20 ± 2 °C. The feed and the permeate were circulated counter-currently at 500 mL/min using two peristaltic pumps. The salt rejection was calculated from the salt concentration of feed and permeate solutions. The permeate flux (J, kg/m^2·h) was calculated using Eqt (2).

$$J = \frac{\Delta W}{A\ \Delta t} \quad (2)$$

where ΔW is the distillation water mass difference (kg), A is the effective area of flat-sheet membrane (m^2), and Δt is the sampling time (h). The rejection coefficient, R (%), was calculated using Eqt (3).

$$R\ (\%) = \left[1 - \frac{C_p}{C_f}\right] \times 100 \quad (3)$$

where C_p is the NaCl concentration of the permeate (g/L) and C_f is the NaCl concentration of the feed (g/L).

2.5. Electrochemical cleaning

The membranes were fouled by the salt solution (3.5 wt% of NaCl) containing surfactant (0.15 mM of SDS) for 5 h and then dried at room temperature for 24 h before the study of electrochemical cleaning [21]. The fouled and dried membranes were then clamped together with a piece of stainless steel wire mesh which worked as the cathode. The other piece of stainless steel wire mesh with the same dimension was placed 1 cm away from the cathode, and the cleaning was initiated using a direct current power supply (Nice Power SPS-305, 0-5 A, 0-30 V) as described elsewhere [22]. The electrolyte was NaCl solution (2 wt%) in the electrochemical cleaning operated at 2V for 1, 2 or 4 min. The water contact angle on the membrane samples before and after electrolysis was measured as described previously. The fouled and cleaned membranes were further evaluated using the DCMD system.

Table 1
The characteristics of the PVDF membrane with different additives.

Membrane	Average thickness						
(μm)	Water contact angle (°)	Sliding angle (°)	Mean roughness (μm)	Mean pore size (μm)	Porosity (%)	Conductivity (1/Ωm)	
PVDF-PMMA	350.4	132.6 ± 1.3	52.9 ± 2.3	0.0919	0.55 ± 0.37	86.4 ± 0.7	0
PVDF-PMMA-CB	343.2	151.5 ± 0.2	6.4 ± 0.6	0.3629	0.12 ± 0.01	82.4 ± 0.2	0.0902
PVDF-CI	257.5	141.4 ± 0.8	29.8 ± 1.1	0.1839	0.16 ± 0.02	85.1 ± 0.2	0
PVDF-PMMA-CI	329.3	149.6 ± 0.7	8.4 ± 0.7	0.2345	0.13 ± 0.01	86.4 ± 0.3	0

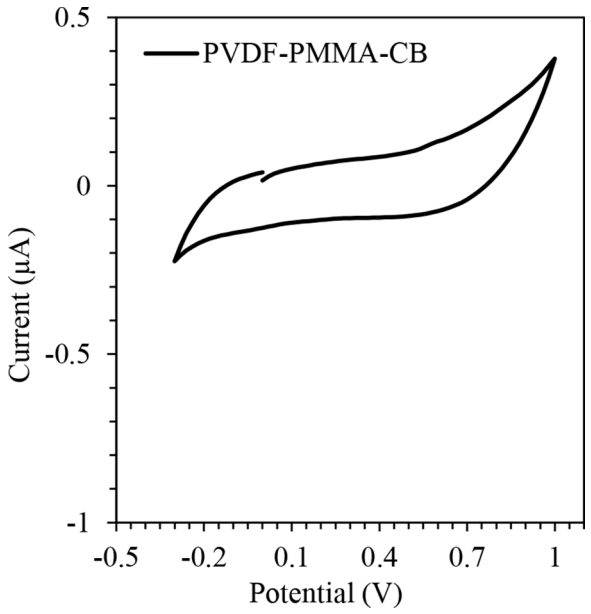

Fig. 4. Cyclic voltammogram for PVDF-membrane with PMMA and carbon black.

3. Results and discussion

3.1. Membrane characteristics

PVDF membranes incorporated with PMMA, carbon black, and/or conductive ink were successfully fabricated. FTIR spectra of different PVDF membranes in Fig. 1 showed similar peaks representing the α-phase of PVDF at 874, 1070 and 1166 cm^{-1}. Meanwhile, the peaks at 836, 1272 and 1400 cm^{-1} were attributed to the β-phase [23,24]. The peaks at 836 and 874 cm^{-1} could be ascribed to C-F stretching vibration and C-C-C asymmetrical stretching vibration, respectively [25,26].

Furthermore, the peaks also appeared at 1166 cm^{-1} (C-C groups), 1272 cm^{-1}, and 1400 cm^{-1} (C-F stretching vibration) [27–29]. The membranes containing PMMA exhibited a peak at 1724 cm^{-1} that represents the C=O stretching vibration [30]. A small peak at band 1666 cm^{-1} could be attributed to C=O stretching vibration of -COOH groups after incorporating carbon black conductive ink [27,31].

All membranes exhibited weave patterns on the surface, as shown in Fig. 2(a)i, (b)i, (c)i, and (d)i. Teoh et al. [19] reported the same imprinting effects of the nonwoven support. The membranes also exhibited porous surfaces with interconnected polymer molecules. However, the surface of the PVDF-PMMA-CB membrane (Fig. 2(c)ii) became rougher than the surface of the PVDF-PMMA membrane (Fig. 2 (a)ii). The incorporation of carbon black particles promoted the formation of pores and secondary roughness on the membrane surface [30, 32]. The PVDF-CI membrane (Fig. 2(c)ii) and the PVDF-PMMA-CI membrane (Fig. 2(d)ii) exhibited less porous and rough surface than the PVDF-PMMA-CB membrane. The cross-sectional SEM images (Fig. 3) reveal the spongy structure with finger-like voids due to the fast solvent exchange rate in the coagulation bath. Incorporating carbon black into the PVDF-PMMA-CB membrane enlarged the diameter of finger-like voids (Fig. 3(b)ii). Mahdavi et al. [32] commented that the strong interaction between PVDF chains with PMMA chains on the carbonaceous surface could delay the phase separation process, resulting in an enlarged void diameter. Comparing PVDF-CI membrane (Fig. 3(c)ii)) and PVDF-PMMA-CI membranes (Fig. 3(d)ii), the length of finger-like voids grew significantly due to the presence of PMMA due to changes in the demixing rate of phase inversion. The velocity of the non-solvent (water) entering the polymer solution and the velocity of the solvent molecules leaving the polymer solution influenced the size of the finger-like void [33]. The hydrophilic PMMA enhanced the pore growth in the PVDF-PMMA-CI membrane because of the increasing demixing rate [30]. The water penetration into the membrane solution was promoted, resulting in pores growth. The membrane thickness in Table 1 was determined using SEM images (Fig. 3). The PVDF-PMMA membrane attained the highest thickness of 350.4 μm. As carbon black was added, the membrane thickness decreased slightly to 343.2 μm. Without PMMA, the thickness of the PVDF-CI membrane was only 257.5 μm. The thickness of the PVDF-PMMA-CI membrane significantly increased to 329.3 μm with the addition of PMMA. The similar finding was reported by Younas et. al [30]. The incorporation of PMMA increased the overall polymer concentration of solution and caused the increment of membrane thickness.

As shown in Table 1, the PVDF-PMMA membrane showed the largest mean pore size with a value of 0.55 μm and the highest porosity of 86.4 %. The mean pore size and porosity decreased significantly with the incorporation of carbon black and conductive ink, as shown by PVDF-PMMA-CB, PVDF-CI and PVDF-PMMA-CI membranes. The pore size and porosity are influenced by the viscosity of the membrane solution [34]. The incorporation of carbon black or conductive ink into PVDF/PMMA and PVDF dope solutions could raise the solution viscosity, delaying the phase separation process. Khalid et al. [35] also reported a similar observation when increasing the loading of dodecylamine modified multi-walled carbon nanotubes. The mean pore size and porosity decreased at the reduced demixing rate when the viscosity of the dope solution was increased.

Table 1 also shows that the PVDF-PMMA membrane exhibited the lowest water contact angle of 132.64 ± 1.3 ° and the highest sliding of 52.9 ± 2.3 ° after achieving the lowest mean roughness. However, the water contact angle on the PVDF-PMMA membrane contact is still higher than the common PVDF membranes due to the micro-roughness created under the templating effect of the nonwoven support [19]. The water contact angle on the PVDF-PMMA membrane is slightly lower than those on PVDF membranes prepared using dual-coagulation baths [36]. The great sliding angle of the PVDF-PMMA membrane (52.9 ± 2.3 °) could be related to the hydrophilic properties of PMMA [30]. As the PMMA was added to the PVDF membrane solution, the dipole-dipole interaction between membrane surface and water molecule was enhanced [37]. The water contact angle could be increased by incorporating carbon black and conductive ink. The PVDF-PMMA-CB membrane attained a superhydrophobic surface and displayed the highest water contact angle of 151.48 ± 0.2 ° and the lowest sliding angle of 6.4 ± 0.6 °. Carbon black particles further enhanced the membrane surface roughness after templating. Hence, the PVDF-PMMA-CB membrane acquired the highest mean surface roughness of 0.3629 μm (Table 1). A similar observation was reported when carbon nanotubes were

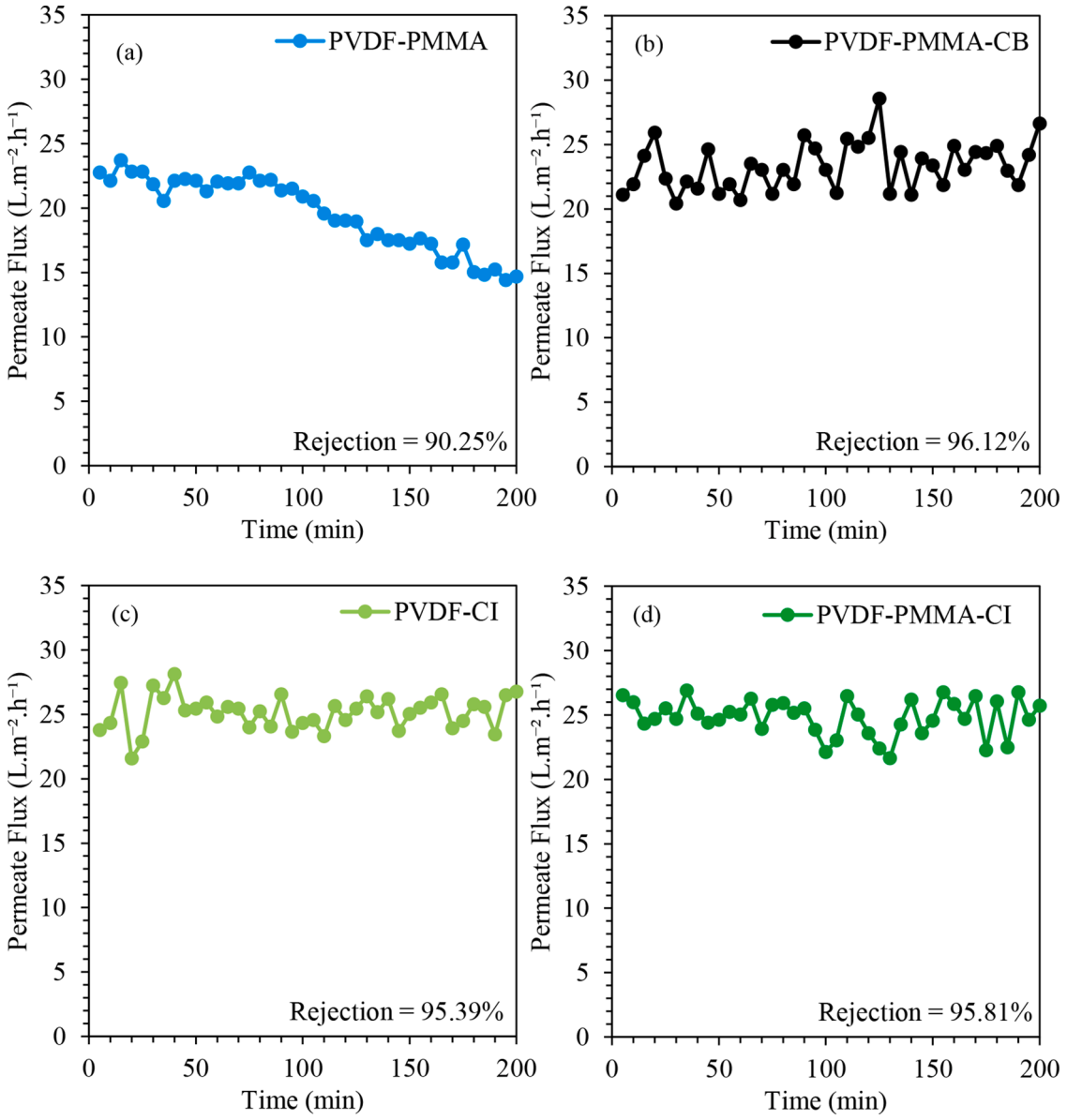

Fig. 5. The permeate flux of (a) PVDF-PMMA, (b) PVDF-PMMA-CB, (c) PVDF-CI and (d) PVDF-PMMA-CI membranes during DCMD of NaCl solution.

incorporated to enhance the surface roughness of polyvinylidene fluoride-co-hexafluoropropylene nanofiber membrane for creating a superhydrophobic surface [38].

The membrane conductivity of the prepared membranes was measured and tabulated in Table 1. However, only the PVDF-PMMA-CB membrane exhibited a very low current with a conductivity value of 0.0902 1/Ωm. This membrane also exhibited a CV curve, as shown in Fig. 4. PVDF-PMMA, PVDF-CI, and PVDF-PMMA-CI membranes are not conductive so they did not generate any reading. The reduction and oxidation of the PVDF-PMMA-CB membrane were successfully improved by incorporating carbon black [39].

3.2. Direct contact membrane distillation (DCMD) performance, membrane wetting, and electrochemical cleaning

In the DCMD test with a feed of NaCl solution (35 g/L), all membranes acquired almost similar permeate flux, near 25.0 L/m^2·h (Fig. 5). However, the permeate flux for the PVDF-PMMA membrane declined after 2 h operation. The flux decline pattern could be related to temperature polarisation and pore wetting [40]. Meanwhile, the permeate flux for other membranes was maintained stable as they are highly hydrophobic.

As shown in Table 2, the water contact angle for all membranes reduced significantly after being wetted with NaCl solution containing surfactant for 5 h. The PVDF-CI membrane experienced the most severe

Table 2
The water contact angle measurement on the PVDF membranes with different additives at different time of electrochemical process.

Electrochemical cleaning duration (min)	Membrane	Water contact angle (°)
0	PVDF-PMMA-E	81.6 ± 0.6
	PVDF-PMMA-CB-E	107.0 ± 0.8
	PVDF-CI-E	75.2 ± 0.3
	PVDF-PMMA-CI-E	75.6 ± 0.4
1	PVDF-PMMA-E1	89.8 ± 0.3
	PVDF-PMMA-CB-E1	129.2 ± 0.1
	PVDF-CI-E1	94.3 ± 0.3
	PVDF-PMMA-CI-E1	99.0 ± 0.5
2	PVDF-PMMA-E2	93.2 ± 0.5
	PVDF-PMMA-CB-E2	135.7 ± 0.6
	PVDF-CI-E2	97.0 ± 0.2
	PVDF-PMMA-CI-E2	123.2 ± 0.4
4	PVDF-PMMA-E4	99.5 ± 0.4
	PVDF-PMMA-CB-E4	148.8 ± 0.3
	PVDF-CI-E4	109.1 ± 0.8
	PVDF-PMMA-CI-E4	131.4 ± 0.6

wetting as the water contact angle reduced from 141.38 ° to 75.2 °. The surfactant in salt solution reduced the interface energy, and the hydrophobic surface of membranes was covered by the hydrophilic groups from the surfactant [41,42]. The water contact angle of the membranes could be restored after electrochemical cleaning by increasing the cleaning time to 4 min. Water contact angles on PVDF-PMMA and PVDF-CI membranes were not fully restored, but the water contact angle of the PVDF-PMMA-CB membrane was effectively restored to 148.8 ± 0.3 °. The PVDF-PMMA-CB membrane is the only conductive membrane in this work. Improving the conductivity of the membrane is essential to enhance electrochemical cleaning [43]. During electrochemical cleaning, the presence of NaCl electrolyte promoted the formation of hypochlorite (OCl^-) and hypochlorous acid (HOCl) to clean the surfactant accumulated on the membrane surface [38]. The stainless steel mesh could transform into insoluble ferric hydroxides at a low concentration to initiate coagulation [44]. The surfactant could be removed through electrostatic absorption followed by coagulation.

After being wetted in the DCMD system with a hot feed containing 35 g/L of NaCl and 0.3 mM of SDS [21], the wetted membranes showed increasing permeate flux (Fig. 6). The permeate flux of the PVDF-PMMA-W membrane increased 8 times compared to the PVDF-PMMA membrane permeate flux due to wetting. Moreover, the salt rejection of the PVDF-PMMA-W membrane was only 2.88% since the liquid instead of the vapour of the feed was transferred through the membrane during wetting. Similarly, the permeate flux for PVDF-CI-W membrane increased up to 300 L/m^2·h with a salt rejection of 6.68% only. The permeate flux decreased gradually after 50 min operation as the feed solution finished. The permeate flux of the PVDF-PMMA-CB-W and PVDF-PMMA-CI-W membranes fell around 60-70 L/m^2·h, with the salt rejection of 10.83% and 5.41% were recorded, respectively (Fig. 6 (b) and (d)). The membrane wetting was induced by the hydrophobic interactions between hydrophobic tails and membrane surface [45]. The hydrophilic head of the surfactant covered the hydrophobic surface of the membranes as the hydrophobic tail of the surfactant interacted with the hydrophobic surface of the membranes.

Then, the wetted membranes were electrochemically cleaned for 4 min before DCMD using 35 g/L of NaCl solution as the feed. The cleaned PVDF-PMMA membrane (PVDF-PMMA-W4) achieved a higher permeate flux than the actual PVDF-PMMA membrane (PVDF-PMMA), with a low salt rejection of 14.27% (Fig. 6(a)). Meanwhile, the permeate flux of the cleaned PVDF-PMMA-CB membrane (PVDF-PMMA-CB-W4) near 15 L/m^2·h was much lower than the permeate of the fresh PVDF-PMMA-CB membrane around 25 L/m^2·h. The salt rejection of the PVDF-PMMA-CB-W4 membrane had been restored to 95.61%, which is near to the satisfactory salt rejection of 99%. For the PVDF-CI-W4 membrane, the permeate flux obtained was 2 times higher than the permeate flux of the fresh PVDF-CI membrane. However, the salt rejection of the PVDF-CI-W4 membrane (46.39%) was only half of the salt rejection of the PVDF-CI membrane. For the PVDF-PMMA-CI-W4 membrane, the permeate flux was recovered, and it is similar to the permeate flux of the PVDF-PMMA-CI membrane (Fig. 6(d)). More importantly, the salt rejection of the PVDF-PMMA-CI-W4 membrane was only slightly affected compared to the PVDF-PMMA-CI membrane.

4. Conclusions

FTIR spectra showed the characteristic peaks of PVDF, PMMA, carbon black and conductive ink. In addition to the microroughness created by the weave, the secondary roughness on the membrane surface was significantly affected by carbon black. PMMA induced finger-like void enlargement during phase inversion after delaying the demixing rate. The absence of PMMA could result in a thin PVDF membrane due to changes in the viscosity of the dope solution. The incorporation of carbon black and conductive ink improved the membrane hydrophobicity significantly, and the PVDF-PMMA-CB membrane even achieved a superhydrophobic surface with a water contact angle of 151.5 ° due to improvement of surface roughness. However, the pore size of PVDF membranes was greatly reduced by incorporating carbon black and conductive ink. The PVDF-PMMA-CB membrane was the only conductive membrane with a CV pattern recorded. Although the PVDF-CI and PVDF-PMMA-CI membranes were not conductive, they attained high permeate flux and salt rejection similar to the PVDF-PMMA-CB membranes. The PVDF-PMMA-CB membrane could be electrochemically cleaned within 4 min after wetting by SDS, showing a recovered water contact angle of 148.8 °. The membrane could be cleaned by hypochlorite (OCl^-), hypochlorous acid (HOCl), and/or ferric hydroxides generated during electrochemical cleaning. The cleaned PVDF-PMMA-CB membrane achieved NaCl rejection of more than 95%, but a slightly lower permeate flux than the permeate flux before wetting. The conductivity of this membrane should be further improved and cleaned through the in-situ electrochemical cleaning process in future works.

Declaration of Competing Interest

The authors declare that they have no conflict of interest.

CRediT authorship contribution statement

N.A. Zakaria: Investigation, Writing – original draft. **S.Q. Zaliman:** . **C.P. Leo:** Conceptualization, Methodology, Writing – review & editing, Supervision. **A.L. Ahmad:** Supervision, Writing – review & editing. **B.S. Ooi:** Funding acquisition, Writing – review & editing. **Phaik Eong Poh:** Investigation, Writing – review & editing.

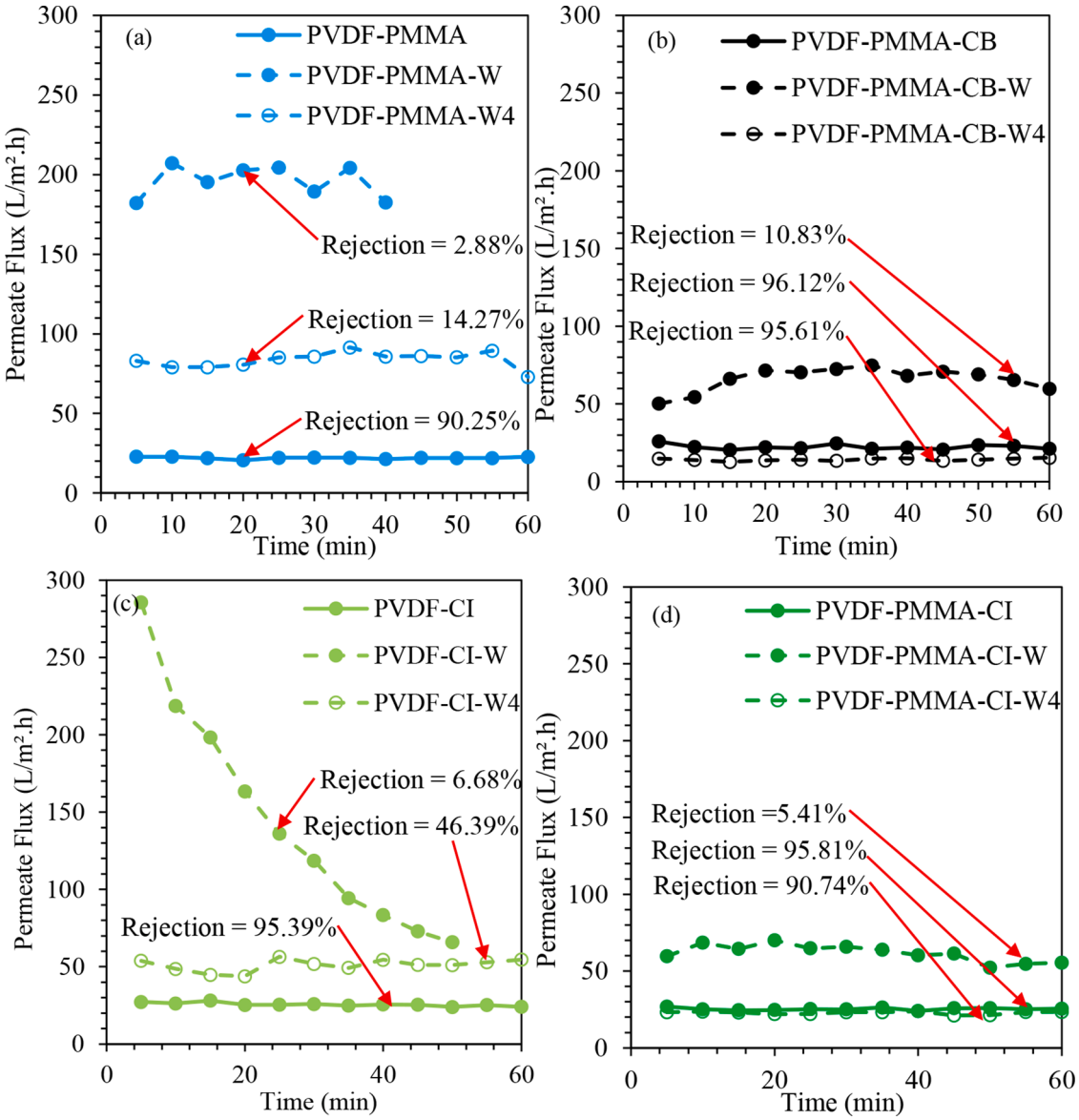

Fig. 6. The permeate flux of (a) PVDF-PMMA, (b) PVDF-PMMA-CB, (c) PVDF-CI and (d) PVDF-PMMA-CI membranes during DCMD of NaCl solution (solid line with solid marker), NaCl solution containing 0.15 mM of surfactant solution (dotted line with solid marker), and NaCl solution using the membrane after 4 minutes of electrochemical cleaning (dotted line with no fill marker).

Declaration of Competing Interest

The authors declare the following financial interests/personal relationships which may be considered as potential competing interests:

B.S. Ooi reports financial support was provided by Malaysia Ministry of Higher Education. C.P. Leo reports financial support was provided by NICT.

Acknowledgements

The authors would like to acknowledge the Ministry of Higher Education Malaysia (LRGS/1/2018/USM/01/1/4; 203/PJKIMIA/67215002) for providing financial support. This work is also the output of the ASEAN IVO (http://www.nict.go.jp/en/asean_ivo/index.html) project, IoT System for Water Reuse in Developing Cities, and financially supported by NICT (http://www.nict.go.jp/en/index.html).

Supplementary materials

Supplementary material associated with this article can be found, in the online version, at doi:10.1016/j.jtice.2022.104448.

References

[1] Wang L, Zang L, Zhang S, Chang J, Shen F, Zhang Y, Sun L. Superhydrophobic fibers with strong adhesion to water for oil/water separation. J Taiwan Inst Chem Eng 2021;131:104166.
[2] Moattari RM, Mohammadi T, Rajabzadeh S, Dabiryan H, Matsuyama H. Reinforced hollow fiber membranes: a comprehensive review. J Taiwan Inst Chem Eng 2021;122:284–310.
[3] Rana D, Bag K, Bhattacharyya SN, Mandal BM. Miscibility of poly(styrene-co-butyl acrylate) with poly(ethyl methacrylate): Existence of both UCST and LCST. J Poly Sci B Polym Phys 2000;38:369–75.
[4] Rana D, Mandal BM, Bhattacharyya SN. Analogue calorimetric studies of blends of poly(vinyl ester)s and polyacrylates. Macromolecules 1996;29:1579–83.
[5] Rana D, Mandal BM, Bhattacharyya SN. Analogue calorimetry of polymer blends: poly(styrene-co-acrylonitrile) and poly(phenyl acrylate) or poly(vinyl benzoate). Polym 1996;37:2439–43.

[6] Rana D, Mandal BM, Bhattacharyya SN. Miscibility and phase diagrams of poly (phenyl acrylate) and poly(styrene-co-acrylonitrile) blends. Polym 1993;34: 1454–9.
[7] Bian X, Huang J, Qiu L, Ma C, Xi D. Preparation, characterization and dyeing wastewater treatment of a new PVDF/PMMA five-bore UF membrane with β-cyclodextrin and additive combinations. Water Sci Technol 2021;283:1847–62.
[8] Shah V, Wang B, Li K. Blending modification to porous polyvinylidene fluoride (PVDF) membranes prepared via combined crystallization and diffusion (CCD) technique. J Memb Sci 2021;618:118708.
[9] Wang D, Zang J, Wang Q, Cheng W, Han G, Huan S. Hierarchical composite membrane with multiscale roughness structures for water-in-oil emulsion separation. Appl Surf Sci 2021;566:150666.
[10] Rajendran S, Mahendran O, Kannan R. Lithium ion conduction in plasticized PMMA-PVdF polymer blend electrolytes. Mater Chem Phys 2002;74(1):52–7.
[11] Ma T, Cui Z, Wu Y, Qin S, Wang H, Yan F, et al. Preparation of PVDF based blend microporous membranes for lithium ion batteries by thermally induced phase separation: I. Effect of PMMA on the membrane formation process and the properties. J Memb Sci 2013;444:213–22.
[12] Tian L, Wang M, Xiong L, Huang C, Guo J, Yao S, et al. Preparation and performance of p(OPal-MMA)/PVDF blend polymer membrane via phase-inversion process for lithium-ion batteries. J Electroanal Chem 2019;839:264–73.
[13] Mondal R, Pal S, Bhalani DV, Bhadja V, Chatterjee U, Jewrajka SK. Preparation of polyvinylidene fluoride blend anion exchange membranes via non-solvent induced phase inversion for desalination and fluoride removal. Desalination 2018;445: 85–94.
[14] Abid HS, Lalia BS, Bertoncello P, Hashaikeh R, Clifford B, Gethin DT, et al. Electrically conductive spacers for self-cleaning membrane surfaces via periodic electrolysis. Desalination 2017;416:16–23.
[15] Yang Y, Qiao S, Jin R, Zhou J, Quan X. A novel aerobic electrochemical membrane bioreactor with CNTs hollow fiber membrane by electrochemical oxidation to improve water quality and mitigate membrane fouling. Water Res 2019;151: 54–63.
[16] Sun J, Hu C, Wu B, Qu J. Fouling mitigation of a graphene hydrogel membrane electrode by electrical repulsion and in situ self-cleaning in an electro-membrane reactor. Chem Eng J 2020;393:124817.
[17] Wei G, Zhao Y, Dong J, Gao M, Li C. Electrochemical cleaning of Fouled laminar graphene membranes. Environ Sci Technol Lett 2020;7:773–8.
[18] Zhang Y, Wang T, Meng J, Lei J, Zheng X, Wang Y, et al. A novel conductive composite membrane with polypyrrole (PPy) and stainless-steel mesh: Fabrication, performance, and anti-fouling mechanism. J Memb Sci 2021;621:118937.
[19] Teoh GH, Chin JY, Ooi BS, Jawad ZA, Leow HTL, Low SC. Superhydrophobic membrane with hierarchically 3D-microtexture to treat saline water by deploying membrane distillation. J Water Process Eng 2020;37:101528.
[20] Hamzah N, Leo CP. Fouling prevention in the membrane distillation of phenolic-rich solution using superhydrophobic PVDF membrane incorporated with TiO_2 nanoparticles. Sep Purif Technol 2016;167:79–87.
[21] Liao X, Wang Y, Liao Y, You X, Yao L, Razaqpur AG. Effects of different surfactant properties on anti-wetting behaviours of an omniphobic membrane in membrane distillation. J Memb Sci 2021;634:119433.
[22] Lalia BS, Ahmed FE, Shah T, Hilal H, Hashaikeh R. Electrically conductive membranes based on carbon nanostructures for self-cleaning of biofouling. Desalination 2015;360:8–12.
[23] Rabuni MF, Nik Sulaiman NM, Aroua MK, Yern Chee C, Awanis Hashim N. Impact of in situ physical and chemical cleaning on PVDF membrane properties and performances. Chem Eng Sci 2015;122:426–35.
[24] Gregorio R. Determination of the α, β, and γ crystalline phases of poly(vinylidene fluoride) films prepared at different conditions. J Appl Polym Sci 2006;100: 3272–9.
[25] Gu S, He G, Wu X, Hu Z, Wang L, Xiao G, et al. Preparation and characterization of poly(vinylidene fluoride)/sulfonated poly(phthalazinone ether sulfone ketone) blends for proton exchange membrane. J Appl Polym Sci 2010;116:852–60.
[26] Bai H, Wang X, Zhou Y, Zhang L. Preparation and characterization of poly (vinylidene fluoride) composite membranes blended with nano-crystalline cellulose. Prog Nat Sci Mater Int 2012;22:250–7.
[27] Silva TLS, Morales-Torres S, Figueiredo JL, Silva AMT. Multi-walled carbon nanotube/PVDF blended membranes with sponge- and finger-like pores for direct contact membrane distillation. Desalination 2015;357:233–45.
[28] Tijing LD, Woo YC, Shim WG, He T, Choi JS, Kim SH, et al. Superhydrophobic nanofiber membrane containing carbon nanotubes for high-performance direct contact membrane distillation. J Memb Sci 2016;502:158–70.
[29] Rahimpour A, Madaeni SS, Zereshki S, Mansourpanah Y. Preparation and characterization of modified nano-porous PVDF membrane with high antifouling property using UV photo-grafting. Appl Surf Sci 2009;255:7455–61.
[30] Younas H, Zhou Y, Li X, Li X, Sun Q, Cui Z, et al. Fabrication of high flux and fouling resistant membrane: A unique hydrophilic blend of polyvinylidene fluoride/polyethylene glycol/polymethyl methacrylate. Polymer (Guildf) 2019; 179:121593.
[31] Lv J, Zhang G, Zhang H, Yang F. Graphene oxide-cellulose nanocrystal (GO-CNC) composite functionalized PVDF membrane with improved antifouling performance in MBR: Behavior and mechanism. Chem Eng J 2018;352:765–73.
[32] Ma W, Zhao Y, Li Y, Zhang P, Cao Z, Yang H, et al. Synthesis of hydrophilic carbon nanotubes by grafting poly(methyl methacrylate) via click reaction and its effect on poly(vinylidene fluoride)-carbon nanotube composite membrane properties. Appl Surf Sci 2018;435:79–90.
[33] Mahdavi H, Zeinalipour N, Kerachian MA, Heidari AA. Preparation of high-performance PVDF mixed matrix membranes incorporated with PVDF-g-PMMA copolymer and GO@SiO_2 nanoparticles for dye rejection applications. J Water Process Eng 2022;46:102560.
[34] Celik Madenli E, Ilkay Ciftci Z. Effects of the carbon nanotube and polymer amounts on ultrafiltration membranes. Environ Eng Res 2021;27:0–3.
[35] Khalid A, Al-Juhani AA, Al-Hamouz OC, Laoui T, Khan Z, Atieh MA. Preparation and properties of nanocomposite polysulfone/multi-walled carbon nanotubes membranes for desalination. Desalination 2015;367:134–44.
[36] Tan HF, Tan WL, Ooi BS, Leo CP. Superhydrophobic PVDF/micro fibrillated cellulose membrane for membrane distillation crystallization of struvite. Chem Eng Res Des 2021;170:54–68.
[37] Ochoa NA, Masuelli M, Marchese J. Effect of hydrophilicity on fouling of an emulsified oil wastewater with PVDF/PMMA membranes. J Memb Sci 2003;226: 203–11.
[38] Tijing LD, Woo YC, Shim WG, He T, Choi JS, Kim SH, et al. Superhydrophobic nanofiber membrane containing carbon nanotubes for high-performance direct contact membrane distillation. J Memb Sci 2016;502:158–70.
[39] Veeramani V, Rajangam K, Nagendran J. Performance of cobalt oxide/carbon cloth composite electrode in energy generation from dairy wastewater using microbial fuel cells. Sustain Environ Res 2020;30:0–7.
[40] Khumalo N, Nthunya L, Derese S, Motsa M, Verliefde A, Kuvarega A, et al. Water recovery from hydrolyzed human urine samples via direct contact membrane distillation using PVDF/PTFE membrane. Sep Purif Technol 2019;211:610–7.
[41] Hakiki F, Maharsi DA, Marhaendrajana T. Surfactant-polymer coreflood simulation and uncertainty analysis derived from laboratory study. J Eng Technol Sci 2015;47: 706–25.
[42] Rezaei M, Warsinger DM, Lienhard JH, Samhaber VWM. Wetting prevention in membrane distillation through superhydrophobicity and recharging an air layer on the membrane surface. J Memb Sci 2017;530:42–52.
[43] Gao C, Liu L, Yu T, Yang F. Development of a novel carbon-based conductive membrane with in-situ formed MnO_2 catalyst for wastewater treatment in bio-electrochemical system (BES). J Memb Sci 2018;549:533–42.
[44] Ahangarnokolaei MA, Ganjidoust H, Ayati B. Optimization of parameters of electrocoagulation/flotation process for removal of acid red 14 with mesh stainless steel electrodes. J Water Reuse Desalin 2018;8:278–92.
[45] Chew NGP, Zhao S, Loh CH, Permogorov N, Wang R. Surfactant effects on water recovery from produced water via direct-contact membrane distillation. J Memb Sci 2017;528:126–34.